Progress in Organic Coatings 210 (2026) 109674

Contents lists available at ScienceDirect

Progress in Organic Coatings

journal homepage: www.elsevier.com/locate/porgcoat

Self-cleaning and antireflection dual-functional gradient-index coatings for enhanced light harvesting in photovoltaic panels

Enyu He [a], Sijie Cheng [a], Rajaram S. Sutar [a], Sanjay Latthe [a,b], Ruimin Xing [a,c], Shanhu Liu [a,*]

[a] College of Chemistry and Molecular Sciences, Henan University, Kaifeng, 475004, PR China
[b] Self-cleaning Research Laboratory, Department of Physics, Vivekanand College (Autonomous), Kolhapur, 416003, Affiliated to Shivaji University, India
[c] College of Energy Science and Technology, Henan University, Zhengzhou, 475004, PR China

ARTICLE INFO

Keywords:
Antireflection
Self-cleaning
Hydroxypropyl cellulose
Photovoltaic panels
SiO_2 coatings

ABSTRACT

Photovoltaic devices are essentially solar collectors that convert incident photons into charge carriers. The development of durable self-cleaning coatings that can effectively reduce light reflection is a key challenge in the use of photovoltaic devices. In this work, a gradient refractive index coating was designed, that reveals both antireflection and superhydrophobic self-cleaning properties. The transmittance of the glass was improved by reducing the light reflection at the air/glass interface. By adjusting coating times of the SiO_2 film, a refractive index gradient interface was optimized. In the range of 300–800 nm, the transmittance of the glass was increased by about 2.0 %–4.7 % at the vertical incidence angle, and the maximum transmittance was increased from 91.6 % to 96.3 %. The self-cleaning experiment of photovoltaic devices verified that the surface could significantly improve the power conversion efficiency. The mechanical stability and environmental aging resistance of the coating were proved through sand impact, outdoor aging, and chemical corrosion tests. This antireflection and self-cleaning coatings technology has broad prospects in the renewable energy sector. Its high light transmittance and superhydrophobic properties can significantly improve the power generation efficiency of photovoltaic modules in challenging environments like deserts areas. It helps to reduce efficiency losses caused by pollution, facilitates effective and sustainable advancements in the photovoltaic industry, and provides essential technical support for the global energy structure upgrade.

1. Introduction

With the rapid development of human society, energy shortages pose a significant challenge due to rising urbanization and technology demands. To sustainably meet future energy needs, researchers must focus on renewable energy sources and enhance energy efficiency. Among the different renewable energy resources, solar energy is one of the most accessible and widely available [1,2]. Extensive research on photovoltaic modules for solar energy utilization has progressed rapidly and attracted considerable global attention. Due to long-term outdoor exposure, dust and foreign substances in the air have a significant impact on the photoelectric conversion efficiency of solar panels [3]. The wetting properties of surfaces play an important role in addressing this issue. Superhydrophilic and superhydrophobic surfaces demonstrate self-cleaning capabilities through water mobility. Superhydrophilic surfaces facilitate self-cleaning by allowing water droplets to spread across the surface and form a thin film. As these droplets spread, they effectively wash away dirt [4,5]. These surfaces are especially advantageous in coastal regions, grasslands, and areas with high humidity and frequent rainfall. They help address issues related to water accumulation from rain or high humidity. However, in low humidity and high dust accumulation situations, the self-cleaning effectiveness of superhydrophilic surfaces will be reduced [6]. Superhydrophobic surfaces facilitate self-cleaning by allowing water droplets to roll off their surfaces. Rolling droplets detach dust particles from the surface, maintaining cleanliness [7]. This property is especially valuable in arid regions, where it reduces dust accumulation and sustains high transmittance, making such surfaces well suited for photovoltaic modules.

In addition, the antireflection films are an indispensable part of most optical and display devices, and have received much attention from researchers because they can effectively enhance the light transmittance [8]. Antireflection films with high-efficiency have been designed and widely applied in anti-fouling [9], optoelectronic materials [10], optical devices [11], and photoelectric conversion [12]. Antireflection films can

* Corresponding author.
E-mail address: liushanhu@vip.henu.edu.cn (S. Liu).

https://doi.org/10.1016/j.porgcoat.2025.109674
Received 24 June 2025; Received in revised form 10 September 2025; Accepted 13 September 2025
Available online 16 September 2025

be classified based on their surface morphology into porous films and dense films. Which may include both single-layer films [13] and multi-layer films [14]. To improve the efficiency of solar cells, single-layer films are usually prepared from materials with low refractive indices including MgF_2 [15], CaF_2 [16], YF_3 [17], TiO_2 [18], SiO_2 [19], and Al_2O_3 [20]. Shen's research group has developed a temperature-controlled method based on dodecylamine (DDA) as a catalyst to prepare hydrophobic monolayer SiO_2 nanonets [13]. Due to the excellent hydrophobicity and chemical inertness of SiO_2 nanonets, they can be used to improve the durability of perovskite solar cells (PSC). The significant improvement in the efficiency of the prepared solar cells proves the stability and universality of SiO_2 nanogrids.

However, single-layer coatings effectively reduce reflections only near specific wavelengths (550 nm) and incidence angles, achieve insufficient reduction, and cannot meet complex requirements or handle specialized substrates. In recent years, the glass coated with double, triple or even more layers of superhydrophobic antireflection coatings can achieve higher transmittance over a wider band (380–800 nm). Xu's research group utilized ZnO nanoparticles as photoluminescent material and SiO_2 sol as the antireflective coatings, which was prepared using multiple impregnation and lifting methods [21]. Different contents of polyethylene glycol (PEG) were added to the ZnO-SiO_2 composite sol to adjust the refractive index of the ZnO-SiO_2 film, which endow ZnO-SiO_2 thin films with antireflection and photoluminescence [22] properties. However, the surface durability [23] and autonomous anti-pollution [24] ability of multi-layer anti-reflective coatings are relatively weak. Therefore, developing materials that integrate both antireflection and self-cleaning [25] functionalities has become a critical research topic.

In this work, the superhydrophobic antireflection coatings was prepared by depositing multiple layers of composite of SiO_2-hydroxypropyl cellulose (HPC) through dip-coating method. While conventional superhydrophobic surfaces often rely on fluorinated or silane-based modifiers to reduce surface energy, the present study achieves superhydrophobicity primarily through hierarchical surface roughness and the inherent surface characteristics of the SiO_2-HPC composite, without the use of any fluorinated compounds. This strategy is consistent with previously reported structure-driven approaches based on the Cassie-Baxter model. Due to the presence of hydrophobic SiO_2 nanoparticles, the resulting coatings exhibits a micro/nanoscale hierarchical surface architecture, which facilitates self-cleaning properties similar to the "lotus effect" [24] seen in lotus leaves. Meanwhile, the coatings showed an antireflection effect to increase the transmittance of sunlight by reducing the light reflection at the air-glass interface. In the spectral range of 300–800 nm, the transmittance of the glass was increased by about 2.0 %–4.7 % at the vertical incidence angle, and the maximum transmittance was increased from 91.6 % to 96.3 %. The self-cleaning and antireflective properties of the coatings prepared on photovoltaics module can significantly improve power conversion efficiency and help maintain the original performance of the device in a complex environment.

2. Experimental section

2.1. Experimental materials

Hydrophobic SiO_2 nanoparticles (Powder, average particle size: 10–15 nm) were obtained from Engineering Research Center for Nanomaterials, Henan University. Hydroxypropyl cellulose (HPC, M.W: 100,000), nitric acid (HNO_3), potassium hydroxide (KOH), anhydrous ethanol was purchased from innochem (Beijing, China).

Glass slides (microscope slides, size: 25 mm × 76 mm × 1 mm) were bought from Beekman (Changde, China). The slides were made of soda-lime glass and were ultrasonically cleaned in ethanol and deionized water before use.

2.2. Preparation of SiO_2-HPC coatings

An SiO_2-HPC antireflection solution was prepared according to the following procedure: A fixed amount of SiO_2 (0.2 g) was dissolved in 50 mL of ethanol solution alongside varying masses of HPC (0.05 g, 0.1 g, 0.2 g, 0.4 g, or 0.6 g). Each mixture was subjected to ultrasonic treatment for 1 h. The resulting solutions were labeled as "SiO_2-HPC-X", where "X" denotes the HPC mass used (e.g., SiO_2-HPC-0.05 for 0.05 g HPC). Based on this screening, the optimal HPC content was determined to be 0.4 g. Subsequently, using this fixed HPC mass (0.4 g), the SiO_2 content was varied (0.1 g, 0.2 g, 0.4 g, 0.5 g, and 0.8 g) in separate preparations. Conditional screening identified the optimal SiO_2 content as 0.1 g. To establish the optimal overall formulation, solutions were prepared with varying SiO_2: HPC mass ratios. The optimal performance was ultimately achieved at a SiO_2: HPC = 1:2.

Commercial glass slides (Lab Shark) were used as substrates. First, the bare glass was cleaned via ultrasonic treatment in water and absolute ethanol for 30 min followed by drying at 70 °C for 24 h. The solution was deposited on the clean glass substrate at a lifting rate of 1000 μm/s through the dip-coating process. After each impregnation, the coatings were dried at 80 °C for 1 h. The samples with different impregnation and lifting times were named SiO_2-HPC-(1−10), respectively. Place the precured coating in a muffle furnace and heat it at a rate of 5 °C/min for 60 min until it reaches a temperature of 300 °C. Keep it at this temperature for 1 h and then cool it to room temperature. The coating fabricated under the optimal conditions (0.1 g of SiO_2, 0.2 g of HPC, 7 dip-coating cycles, calcination at 300 °C) was designated as SiO_2-HPC.

2.3. Stability test

The mechanical durability of the prepared coating was evaluated through sandpaper wear test; water drop impact test and sand grain impact test.

Sandpaper wear test: A weight of 20 g was placed on the coated glass sample, which was held firmly against the sandpaper. The sandpaper was then moved in a reciprocating motion, with the sandpaper rubbing against the coatings. Each wear cycle involved moving the sample 8 cm forward and 8 cm backward along a ruler. The water contact angle (WCA) of the sample was measured after each wear cycle.

Water droplet test: A total of 1500 mL of water droplets was continuously dropped onto the inclined sample surface at an angle of approximately 45° from a height of 40 cm. The volume of each droplet was approximately 120 μL. The WCA of the sample was measured after every 300 mL of water was applied.

Sand grain-dropping test: 300 g of sand were dropped from a height of 80 cm, and effected surface area of the coatings was tested by measuring WCA.

Outdoor aging test: The coated glass substrate was placed in an outdoor open space to test their natural environment resilience. The experiment was conducted on the rooftop of the College of Chemistry and Molecular Sciences at Henan University (from February 15, 2025 to March 12, 2025 and from July 31 to August 13, 2025). During the test, the transmittance and WCA were measured daily to analyze the durability of the film.

2.4. Application of SiO_2-HPC coatings on PSC

The photocurrent density-voltage characteristics of the PSCs were measured using a CHI-760 source measurement unit and a solar simulator (Perfect Light Ltd., PLS-SXE 300, China). The light intensity of the solar simulator was set to 1000 $W{\cdot}m^{-2}$. The devices were measured at a scan rate of 24 $mV{\cdot}s^{-1}$. The active area of the device was 25 cm^2.

Two identical 1.5 W commercial monocrystalline silicon solar panels, one with the SiO_2-HPC coatings applied and the other with a bare glass surface were placed outdoors, and their voltage and current were recorded hourly. The energy output was calculated to evaluate the effect

of the coatings.

2.5. Characterization of SiO_2-HPC coatings

The surface morphology of the SiO_2-HPC coatings was observed by field emission scanning electron microscope (FESEM, JEOL JSM-7610F, Japan), and elemental composition was analyzed by energy dispersive X-ray spectroscopy (EDS). The water contact angle (WCA) was measured using a contact angle goniometer (Zhongchen, SCI60000E, China), where 8 μL of deionized water was dropped on the film surface, and the angle was recorded. UV–vis-NIR spectra in the range of 300–800 nm was recorded using a spectrophotometer (Agilent, TY2021006984, China). The infrared spectra of the coatings were obtained using a Fourier-transform infrared spectrometer (FT-IR, TENSOR II, Germany). Dynamic droplet motion images were recorded using a high-speed camera (PHOTRON, PFV-4, Japan). Surface topography was assessed by atomic force microscopy (AFM, Oxford Instruments), with a scan area of 5 × 5 μm. Samples such as dry freestanding pristine Low-Density Polyethylene and Self-Assembled Thin film were affixed to the sample stage using double-sided carbon tape.

3. Results and discussion

3.1. Structural and chemical analysis of SiO_2-HPC coatings

Fig. 1a illustrates the dual-function SiO_2-HPC coatings on a photovoltaic glass surface, which achieves enhanced light transmittance and helps reduce dust accumulation by virtue of its self-cleaning effect under outdoor conditions. Due to the presence of reactive groups and excellent adhesion, HPC was selected as the functional layer. The thickness and refractive index of the coatings were optimized by adjusting the concentration of the coating solution, the rate of dipping and lifting, and the annealing temperature. This the researchers allows to control the wetting and antireflection properties of the coatings effectively. As shown in Fig. S1, SiO_2 nanoparticles form a uniform layer on the glass surface using the dipping method. Moreover, porous SiO_2 antireflection coatings can be created after removing cellulose through annealing. This is confirmed by scanning electron microscopy (SEM) analysis Fig. 1b illustrates the uniform distribution of SiO_2 nanospheres on the glass substrate. The thickness of the silica nanonet and the corresponding energy spectrum analysis are shown in Fig. S2-S3. As can be seen from

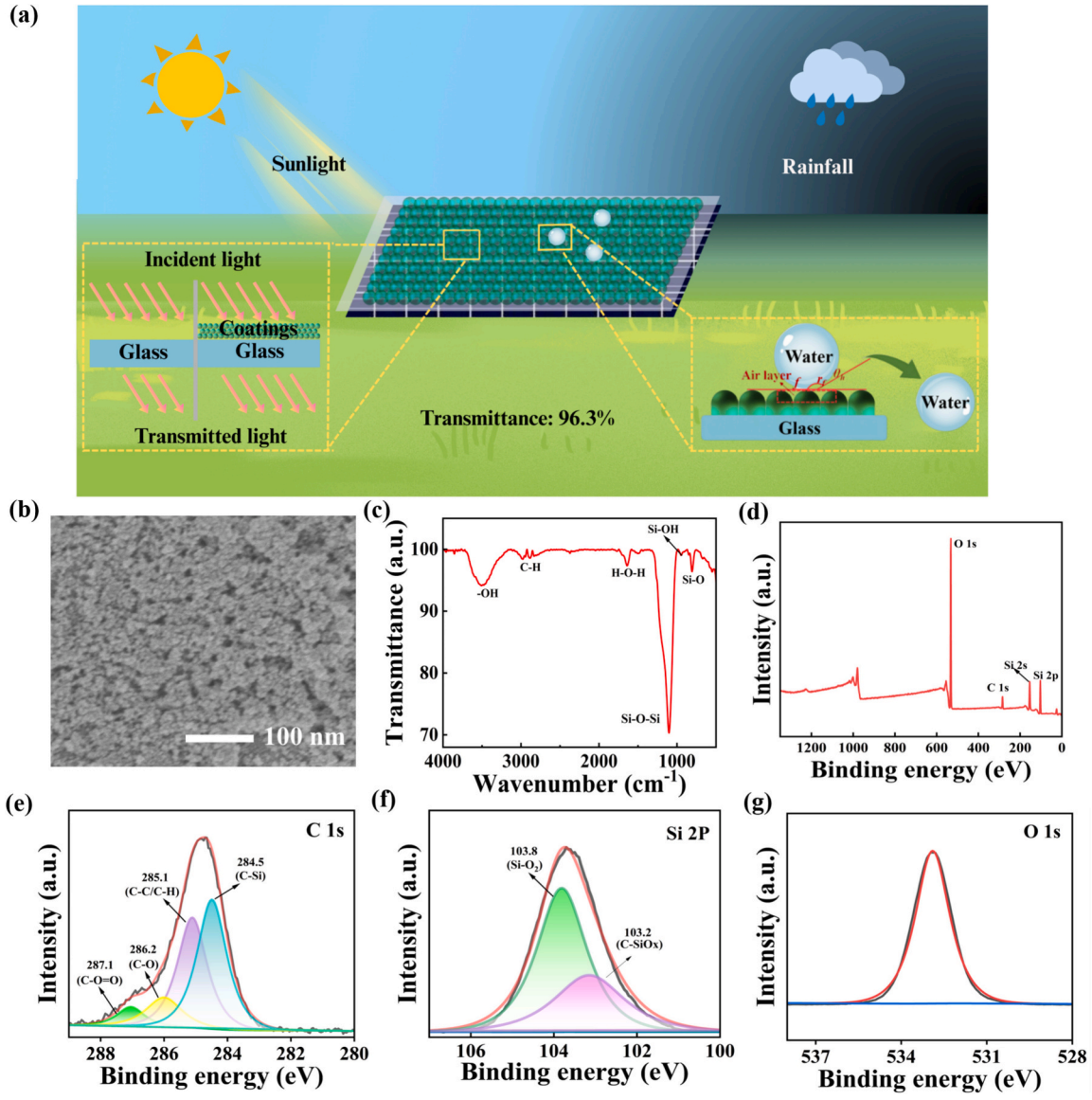

Fig. 1. (a) Schematic diagram depicting the antireflection and self-cleaning features of a solar panel. (b) SEM images of the prepared SiO_2-HPC coatings. (c) FT-IR of SiO_2-HPC coatings. (d) XPS survey of SiO_2-HPC coatings. High-resolution spectra of (e) C 1 s spectra, (f) Si 2p spectra and (g) O 1s spectra.

the figure, the uniform arrangement of the coating obtained by dip-coating forms a SiO_2 nano-network with a certain thickness.

The FT-IR spectrum of the SiO_2-HPC coatings is shown in Fig. 1c. A strong and broad absorption band at 1113 cm^{-1} corresponds to the antisymmetric stretching vibration of Si-O-Si bridges within the silica network, where one Si—O bond elongates while the other contracts. [26]. The peak at 811 cm^{-1} is attributed to the symmetric stretching mode of Si—O. A broad band centered at 3496 cm^{-1} is associated with the O—H stretching vibration of surface hydroxyl groups and adsorbed water, typically broadened due to hydrogen bonding. The peak near 1635 cm^{-1} is assigned to the bending vibration of molecular water (H-O-H) [22], while the band at 972 cm^{-1} is attributed to Si-OH groups present on the silica surface, indicating surface hydroxylation. Moreover, the XRD analysis indicates that both types of SiO_2, before and after annealing, exhibit an amorphous structure (as shown in Fig. S4).

The surface chemical properties of SiO_2-HPC were further investigated using XPS spectroscopy. The full scan XPS spectra for SiO_2-HPC coatings, as well as the deconvoluted spectra for O 1 s, C 1 s, and Si 2p, are shown in Fig. 1d-g, respectively. In the C 1 s spectrum, two broad peaks appear at 285.1 eV and 286.2 eV [14], corresponding to the C—C bond and the C—O group, respectively (Fig. 1e). The Si 2p spectrum displays two broad peaks at 103.8 eV and 103.2 eV (Fig. 1f), which correspond to SiO_2 and C-SiOx. The O 1 s spectrum (Fig. 1g) shows a relatively broad peak, which is associated with the O—Si bond in the inorganic phase and the O—C bond in the hydroxyl group (532.8 eV) [27]. XPS analysis showed that, after annealing (Fig. S5), the C 1 s signal was markedly reduced, indicating removal of organic residues, whereas the Si 2p and O 1 s peaks became more prominent and better resolved [28]. Such compositional changes are consistent with the formation of a uniform and stable SiO_2 network, which may contribute to the observed improvements in wetting resistance and optical performance.

3.2. Optical properties of SiO_2-HPC coatings

The visual evidence of antireflection capabilities of coated and uncoated glass is shown in Fig. 2a. The SiO_2-HPC coated glass (upper panel) shows clear visibility of text in contrast to the obscured text seen for uncoated glass (lower panel). The influence of SiO_2 concentration and HPC content on the antireflection properties of SiO_2-HPC coatings was systematically investigated. As shown in Fig. 2b-e, the transmittance of the coated samples demonstrates significantly enhanced performance compared to bare glass substrate, confirming the inherent

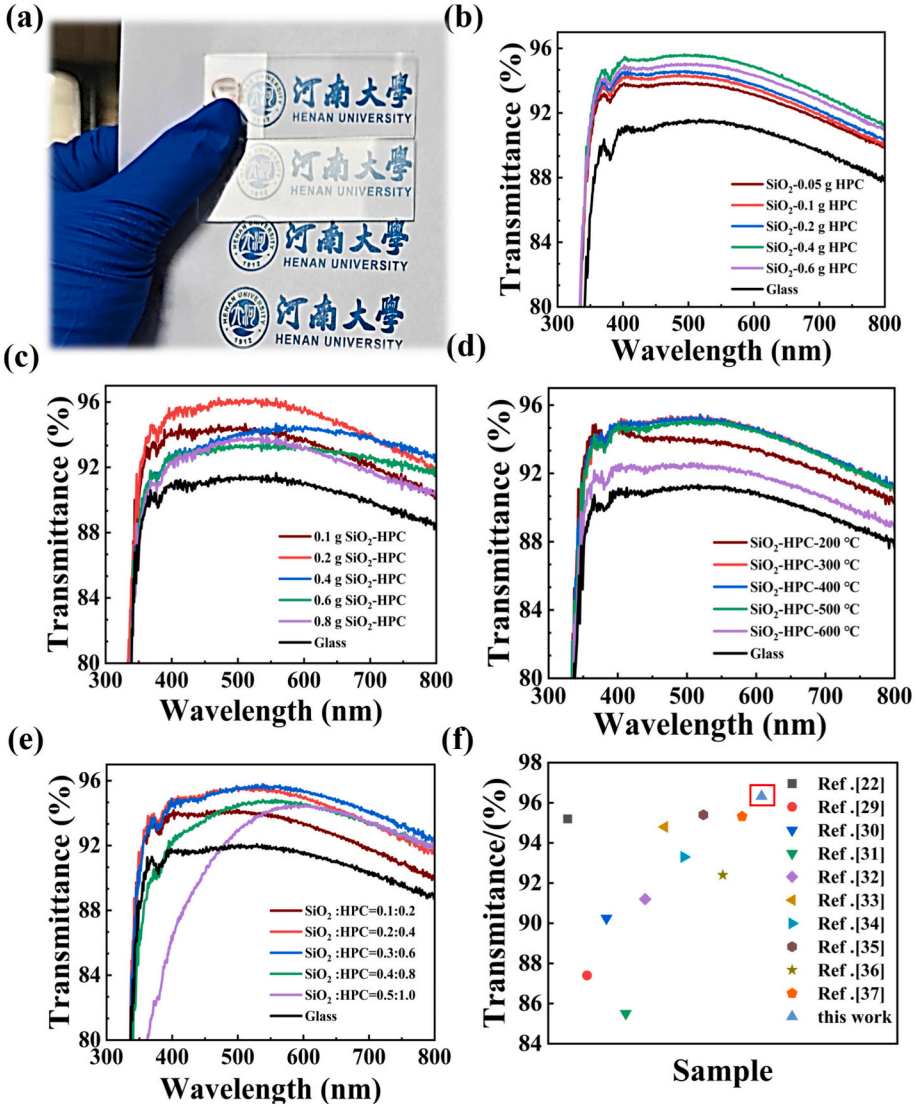

Fig. 2. (a) Comparison of antireflection between uncoated glass substrate (bottom) and SiO_2-HPC-coated glass (top). Relationship of transmittance of SiO_2-HPC coated glass with varying content of (b) HPC; (c) SiO_2; (d) Ratio of SiO_2 to HPC; and (e) Annealing temperature. (f) Comparison of transmittance with previous literature.

antireflection properties of the SiO_2-HPC coatings. Notably, the reflectance of the coated glass substrate was markedly reduced compared to bare glass substrates, which exhibiting approximately 91.6 % reflectance. Fig. 2b indicates that the substrate's transmittance follows a parabolic trend based on HPC content, with maximum transmission occurring at an HPC concentration of 0.2 g. Fig. 2c and d explore the relationship between the mass ratio of SiO_2 and HPC, with an optimal ratio of 1:2. From the data, it can be concluded that the coatings demonstrate the highest transmittance when the mass ratio is maintained at 1:2.

Furthermore, we investigated the impact of annealing temperature on optical performance, finding that samples annealed at 300 °C demonstrated superior transmittance (Fig. 2e). As illustrated in Fig. S6, the transmission spectra of glass substrates coated with different numbers of antireflection layers (ranging from 5 to 9 dips) showed a progressive enhancement in performance, achieving a peak transmittance of 96.3 % at seven coating layers compared to a baseline transmittance of 91.6 %. This significant improvement can be attributed to the nanoscale porosity within the SiO_2-HPC layers, which effectively reduces the effective refractive index. A quantitative comparison with recent superhydrophobic surfaces (shown in Fig. 2f and Table S1) indicates that the UV–visible light transmittance (300–800 nm) of the coatings developed in this study exceeds that of previously reported antireflection and self-cleaning coatings [22,29–37]. The performance enhancement likely results from the synergistic effects within the multilayer architecture, which collectively reduces surface reflectance.

The effect of film surface roughness on transmittance exhibits a double-edged sword characteristic [38]. When the surface root mean square (RMS) is less than 1/10 of the incident wavelength, following the Rayleigh scattering criterion [39], surface scattering can be ignored. Notably, by constructing a gradient refractive index interface, surface roughness can be transformed into an optical advantage. The surface micro-nano structure was created by depositing SiO_2-HPC onto glass substrates and then annealing them. This resulted in a root mean square (RMS) roughness of 47.69 nm (Fig. 3a). The rough texture of SiO_2-HPC can trap air, forming a composite interface that significantly increases the apparent WCA (Fig. 3b). Gradient refractive index coatings, which were developed through geometric control, can maintain excellent optical performance even under complex working conditions.

According to the effective medium theory (EMT) [40,41], the micro-nanostructure can be approximated as an equivalent medium film consisting of multiple layers with varying refractive indices, and each layer exhibited a gradient in refractive index. By introducing buffer layers with gradually decreasing refractive indices (ranging from approximately 1.53 to 1.0) at the air/glass interface, a smooth gradient refractive index profile can be established, thereby reducing Fresnel reflections. As shown in Fig. 3c, porous SiO_2 films were prepared and served as antireflection layers. The refractive index was tailored by modulating the porosity through the controlled deposition of SiO_2 nanoparticles. This relationship is described by the following EMT-based equation:

$$n_p^2 = (n_s^2 - 1)(1 - p) + 1$$

where n_p and n_s represent the effective refractive index of the porous material and the intrinsic refractive index of the solid matrix, respectively, and p denotes the porosity. With successive layer-by-layer deposition of SiO_2 nanoparticles, surface roughness and effective porosity increased due to the buildup of loosely packed hierarchical structures. According to EMT [41], the loosely packed hierarchical structures provide more voids and increases the air fraction, resulting in a gradual decrease of the effective refractive index. The optimized SiO_2 film exhibited a refractive index of approximately 1.14 at 550 nm, which close to the ideal single-layer antireflection index of 1.23.

To further investigate the antireflection performance of the SiO_2 film, the thickness was varied by adjusting the concentration of the SiO_2 mixed solution. Cross-sectional SEM analysis (Fig. S2) revealed that the highest transmittance was achieved after annealing at a film thickness of 23 μm. A comparison was made between the transmittance of the glass substrate without the SiO_2 film and with the optimized mesoporous SiO_2 film. Within the spectral range of 300 to 800 nm, the transmittance of the substrate was successfully increased by approximately 2.0 % to 4.7 %. By applying the porous SiO_2 antireflection film, the maximum transmittance improved from 91.6 % to 96.3 %.

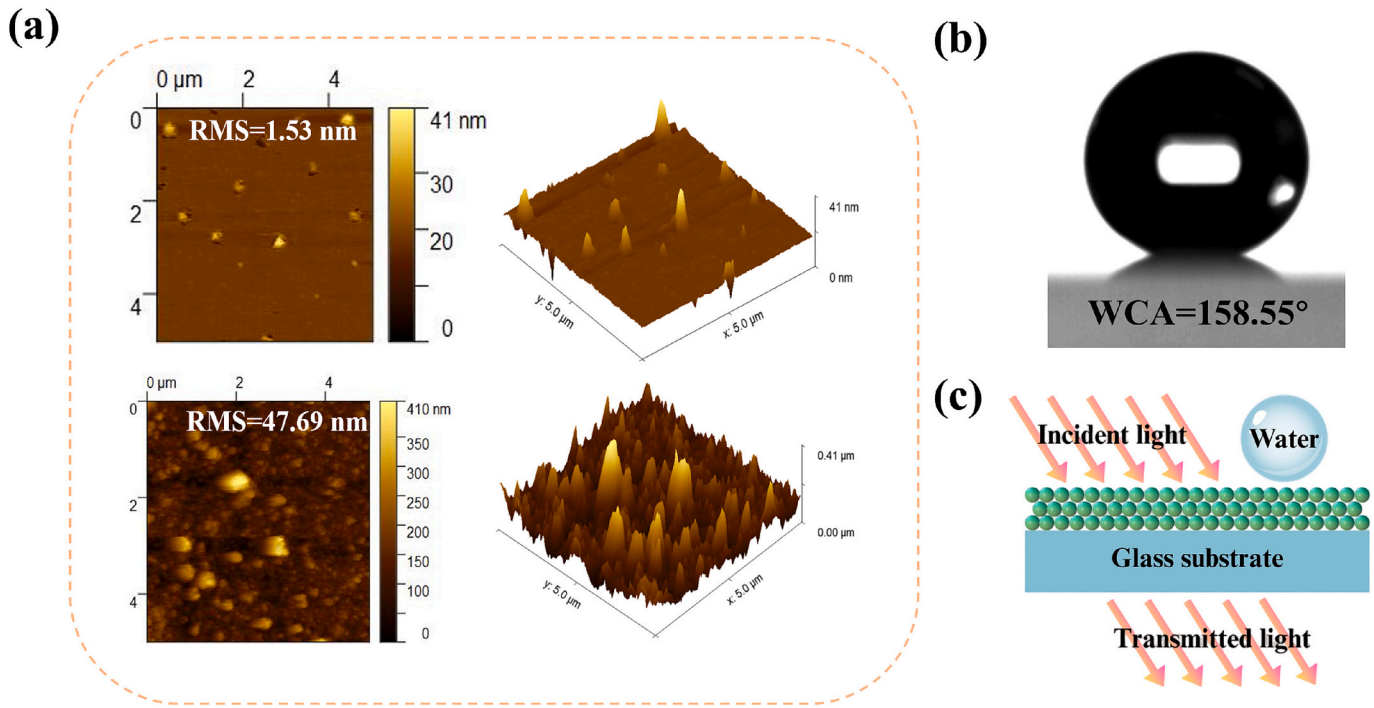

Fig. 3. (a) Atomic force microscope images of bare glass (top) and coated glass. (b) Schematic diagram of the contact Angle on the coatings surface. (c) Principle of antireflection coatings.

3.3. Self-cleaning performance of SiO_2-HPC coatings

The formation of a superhydrophobic surface relies on the rough structure created by a dense arrangement of hydrophobic nano-silica particles. The resulting SiO_2-HPC coatings exhibit excellent superhydrophobicity and low adhesion to water droplet. The SEM image of the surface (Fig. S7) shows that the coatings are both porous and dense, featuring a micro and nanoscale composite rough structure. Fig. 4a displays the WCA for coatings with varying SiO_2 content, revealing that the coatings do not achieve superhydrophobicity when the SiO_2 content is extremely low. In addition, WCA were measured for coatings with different application times and annealing temperatures (Fig. S8-S9). When the coating times were set at 1–2, the WCA indicated that superhydrophobicity was not achieved, likely due to the low SiO_2 content in the coating layer. However, with coating times of 9–10, hydrophobicity decreased because of an uneven coating surface. This suggests that the structural influence on the WCA of the coatings is quite significant.

The annealing temperature has a significant impact on the surface structure of coatings. Insufficient annealing temperature may leave residual hydroxyl groups or bound water on the film surface and hinder the development of the necessary micro/nanostructure for superhydrophobicity, resulting in lower WCA (Fig. S9–10). Conversely, if the annealing temperature is too high, the silica structure can collapse, preventing the formation of a superhydrophobic surface. To develop transparent superhydrophobic coatings, it is essential to consider the roughness of the coating's surface, control the coating thickness, and use low surface energy substances. The remarkable roughness and strong hydrophobicity of the SiO_2-HPC coatings ultimately lead to the creation of effective self-cleaning and anti-reflective coatings. As shown in Fig. 4b, when water droplets deposit on the contaminated glass surface, they tend to stick to the surface due to strong adhesive interactions between the liquid and solid phases. This adherence limits the movement of the droplets and hinders their effectiveness in removing surface contaminants through rolling of water droplets. However, when water droplets fall onto the contaminated surface of glass coated with SiO_2-HPC, they roll off while carrying the contaminants with them. Further evidence of the low interfacial adhesion force between the SiO_2-HPC coated glass and the water droplets is provided by high-speed camera footage that captures the dynamic and continuous rebound behaviors. The droplet bounce process occurs within a span of just 41 ms and is illustrated in Fig. 4c. Notably, the water droplets rebound four times on the SiO_2-HPC coating within 200 ms before rolling off freely.

Further, conducting quantitative self-cleaning experiments with small airborne particles is challenging due to their variability in size and composition. To address this, previous studies have employed model contaminants such as sea sand (100–300 μm), carbon nanotubes (10 μm), fly-ash (45 μm), and red clay (25 μm) [42]. In this study, fluorescent microspheres (size of 38 μm) were selected as representative particles to evaluate the self-cleaning performance of the SiO_2-HPC coating under simulated environmental conditions. These microspheres offer uniform size, strong fluorescence under UV light, and high visibility, especially under low-light conditions. As shown in Fig. 4d, fluorescent particles were evenly distributed on both bare and coated glass substrates. After xenon lamp illumination on this surface, simulated cleaning with deionized water droplets, the uncoated glass substrate retained significant particle residue due to stick of water droplets on its surface, in contrast the SiO_2-HPC surface showed clean. This enhanced self-cleaning performance is attributed to the synergistic effect of superhydrophobicity. The high WCA facilitated droplet rolling,

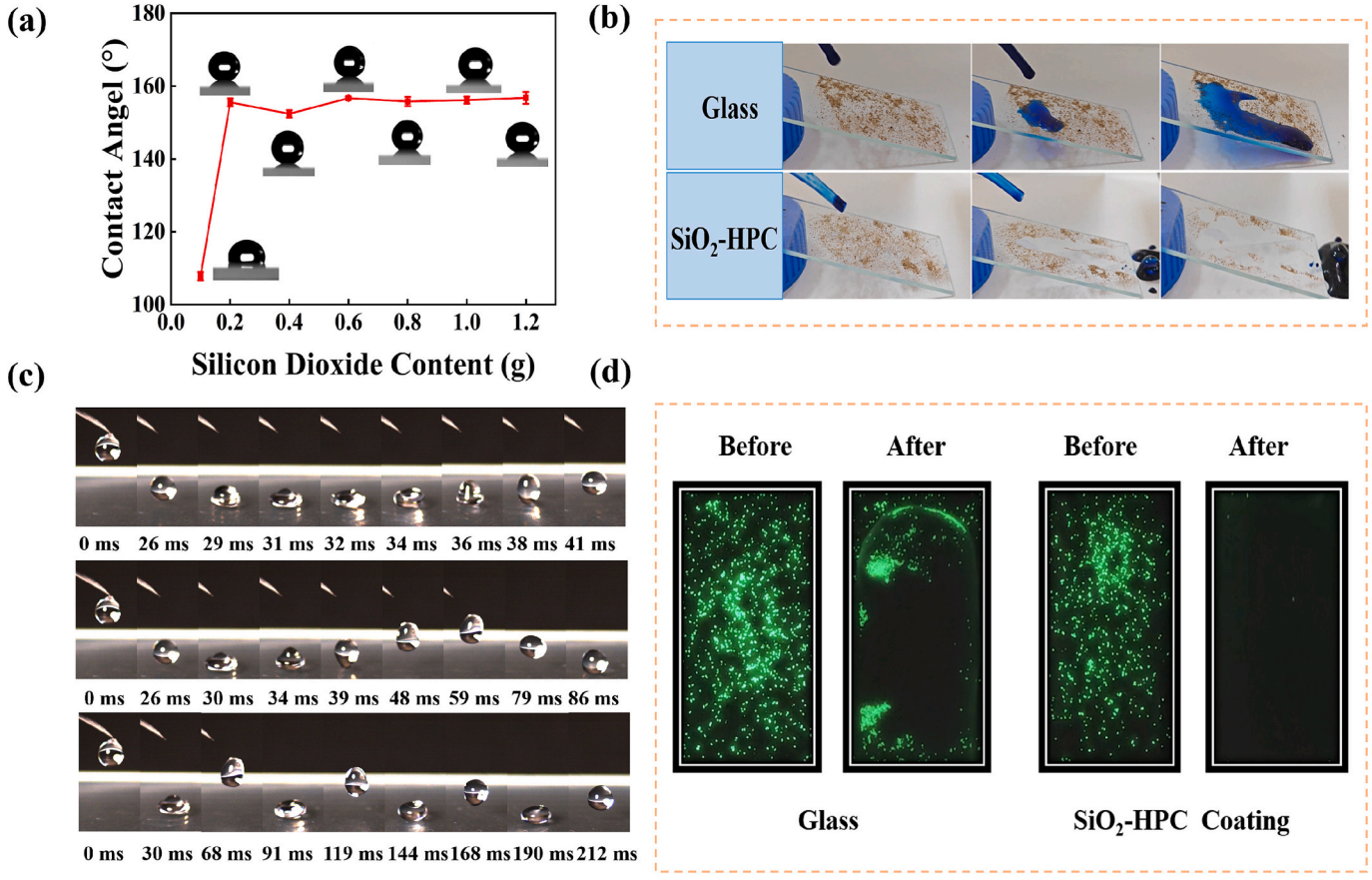

Fig. 4. (a) WCA of coatings with different SiO_2 content. (b) Self-cleaning performance in multi-sedimentation environments. (c) The bouncing process of water droplets captured by high-speed cameras. (d) Self-cleaning performance of small particle pollutants.

effectively dislodging particles. Moreover, the low surface energy and trapped air pockets reduced particle adhesion. These results confirm the excellent self-cleaning ability of the SiO_2-HPC coatings and their potential for outdoor applications.

3.4. Stability of SiO_2-HPC coatings

Strong adhesion, mechanical robustness and environmental durability are crucial for the application of anti-reflective superhydrophobic coatings in outdoor solar panels and architectural glass. SiO_2-HPC-coated glass was subjected to outdoor exposure tests that simulate real-world aging conditions to evaluate its stability (Fig. S11). The transmittance and WCA of the coated glass were periodically measured during 42 days outdoor aging test (on days 1–7, 14, 21, 28, 35 and 42). As shown in Fig. 5a-b, the coatings maintained excellent optical performance, with transmittance at 550 nm remaining stable at approximately 95.8 %. Likewise, the WCA (Fig. S12,13) exhibited minimal change, confirming strong resistance to environmental degradation. The transmittance at 550 nm declined by less than 1.5 %, and the WCA remained above 146°, indicating that the coatings retained high hydrophobicity and excellent optical transparency. The slight decrease in WCA is may be due to prolonged UV exposure and environmental contaminants, which may partially degrade the low surface energy components and slightly damage the hierarchical surface structures of SiO_2-HPC coatings. These results confirm that the SiO_2-HPC coatings possesses remarkable environmental durability, and is highly suitable for practical outdoor applications. The chemical resistance of the coatings was further examined by exposing them to solutions with varying pH levels (1,7 and 14) (Fig. 5c-d). The WCA in acidic conditions was slightly lower than in neutral water, likely due to partial penetration of the solution into the micro/nanostructure or mild protonation of surface groups, such as the formation of Si-OH. In alkaline environments, the WCA decreased more significantly, possibly due to surface swelling or slight corrosion-induced that include changes in roughness. This moderate hydrophobicity, even after structural degradation, is likely due to a transition from the Cassie-Baxter state to a metastable Cassie-like regime, where partial air entrapment contributes to water repellency. Notably, the coatings retained their structural integrity without a complete loss of functionality. These findings demonstrate that SiO_2-HPC coatings exhibit outstanding stability, making it highly suitable for long-term outdoor applications.

The mechanical durability of the SiO_2-HPC coatings was evaluated using sand impact tests, with WCA and optical transmittance as performance indicators (Fig. 5e-f). After exposure to 300 g of sand, the coatings maintained a high transmittance at 550 nm (95.6 %) and a WCA of 146.66°, demonstrating strong resistance to mechanical abrasion. This robustness is attributed to the synergistic effects of hierarchical micro/nanostructures and strong interfacial interactions both within the composite and at the coating substrate interface [38]. The measured RMS roughness of 47.69 nm supports a Cassie-Baxter wetting state by trapping air pockets, minimizing solid-liquid contact and reducing particle adhesion. Condensation reactions between surface silanol groups and hydroxyl groups on the glass substrate form stable Si-O-Si covalent bonds. This dual mechanism of chemical bonding and mechanical interlocking ensures a robust interface [34], effectively preventing coatings delamination under mechanical impact and thereby validating the claimed mechanical stability. Further durability tests were conducted, including exposure to 1500 mL of water (Fig. S14), fifty cycles of sandpaper friction (Fig. S15), and images showing various pollutants on the coatings (Fig. S16). The coatings resilience against sand impact and sandpaper abrasion is attributed to the cohesive network formed by HPC and SiO_2 nanoparticles, which dissipates mechanical energy. This design capitalizes on the mechanical strength of SiO_2 and the flexibility of HPC, achieving a balance of optical, mechanical, and chemical robustness. These findings suggest significant potential for enhancing the optical transparency and long-term durability of devices such as solar photovoltaic panels and architectural glass.

3.5. Device performance evaluation

The parameters of the SiO_2-HPC antireflection coatings discussed in this paper aim to enhance the power conversion efficiency (PCE) and short circuit current density (JSC) of open circuit voltage (OCV) by minimizing surface Fresnel losses. We prepared glass with (treated) and without (control) SiO_2-HPC films for use in solar cells. The power conversion efficiency and internal resistance of solar cells are influenced by the size and conductivity of the cells, and larger solar cells may experience decreased PCE due to potential defects.

In this study, we used a smaller size solar cell (5 cm × 5 cm) for performance evaluation. The small area device was cut from the same larger solar cell to reduce performance variation. Fig. 6a illustrates the device's current density-voltage (J-V) curve recorded at 0° (vertical incidence) under 1000 $W{\cdot}m^{-2}$ irradiation. The current density was calculated based on the effective area of the device to assess the impact of the antireflection film on performance. The statistical photovoltaic (PV) parameters of these devices include VOC, JSC, fill factor (FF), and PCE (Fig. 6b-d). The average JSC increased from 3.76 mA/cm^2 to 4.05 mA/cm^2, marking an increment of 0.23 mA/cm^2. The VOC and FF of both the control and treated devices were comparable, resulting in an average increase in PCE from 4.81 % to 5.21 %. The introduction of SiO_2-HPC coatings decreases the substrate's reflectivity and increases its transmittance, thereby enhancing both JSC and PCE. To assess the practical performance of the SiO_2-HPC coatings, a side-by-side outdoor test was conducted using two identical commercial solar panels, with one panel bearing the SiO_2-HPC coatings and the other remaining uncoated. Under typical outdoor conditions with high temperatures and intense sunlight, the coated panel consistently delivered higher power output than the uncoated reference. Outdoor energy output data (Fig. 6e) indicate that the SiO_2-HPC coated solar panel exhibited an average energy output that was 5.64 % higher than that of the uncoated panel. This improvement can be attributed to the coating's self-cleaning capability and antireflective properties, which prevents the accumulation of dust and reduce light reflection, respectively. These effects improve the overall photovoltaic efficiency of the coated solar panel under real-world conditions, demonstrating the potential of SiO_2-HPC coatings for outdoor applications.

4. Conclusion

In summary, we developed dual-functional coatings through the sequential deposition of SiO_2-HPC multilayers using a dip-coating technique that provide both antireflection and self-cleaning properties. The hierarchical micro-nano architecture of the SiO_2 particles creates a graded refractive index profile, which enhances surface roughness while maintaining optical clarity. The optimized coatings achieve 96.3 % transmittance which represents a 4.7 % absolute gain over bare glass while exhibiting superhydrophobicity (WCA = 158.55°). Rigorous durability assessments, including water impact, sand abrasion resistance, chemical corrosion exposure, and long-term outdoor aging demonstrate exceptional mechanical robustness and environmental stability. Importantly, the coatings maintain their self-cleaning functionality even under sustained harsh conditions. These synergistic properties make them suitable for integration with photovoltaic systems, where light-trapping efficiency and contamination resistance are crucial. These results demonstrate significant commercial potential for SiO_2-HPC coatings in generation solar energy applications.

CRediT authorship contribution statement

Enyu He: Writing – original draft, Methodology, Investigation, Data curation. **Sijie Cheng:** Writing – original draft, Investigation, Data

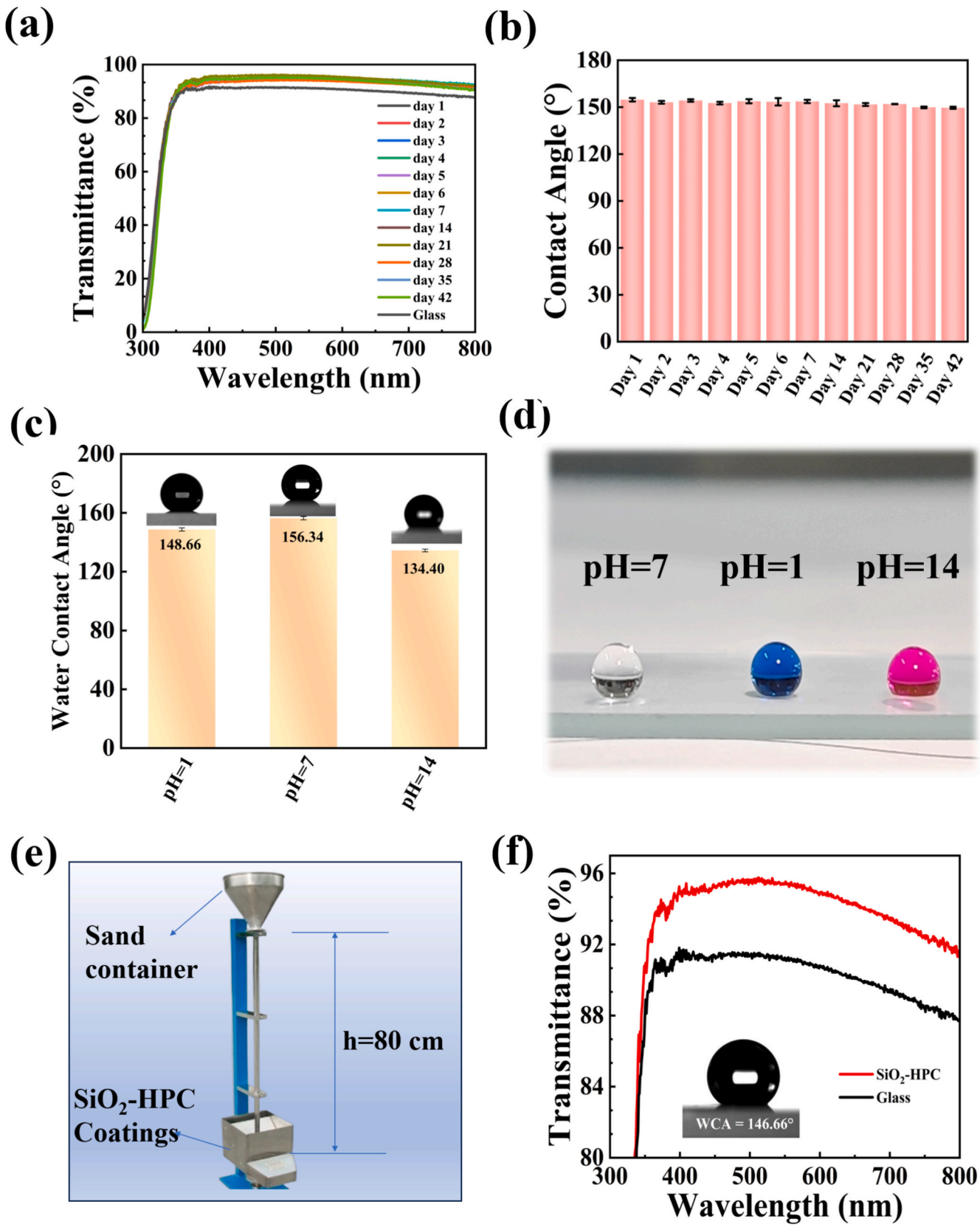

Fig. 5. Durability of the anti-reflective coatings. (a) Ultraviolet spectra with different outdoor aging times. (b) WCA for different days of aging. (c-d) WCA and physical images of liquid droplets with different pH on the coatings. (e-f) Schematic diagram of the sand-dropping test, transmittance and WCA of the coatings after the sand-dropping test.

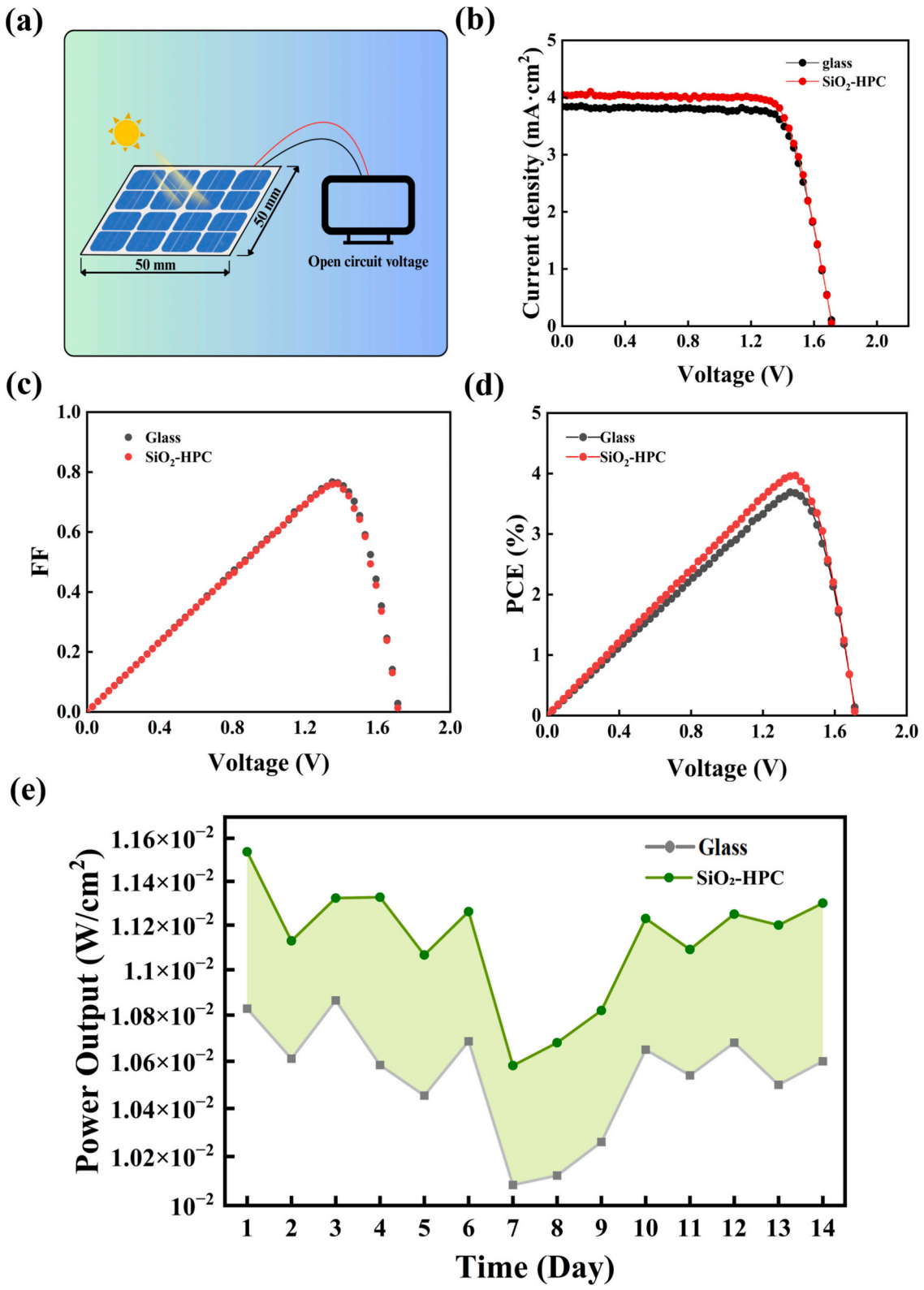

Fig. 6. (a) Schematic diagram of the device encapsulated with antireflection film. (b) The J-V curve of the device encapsulated with antireflection film. (c) The FF of the device encapsulated with antireflection film. (d) The PCE value of the device encapsulated with antireflection film. (e) 1–14 days energy output of SiO_2-HPC coatings and uncoated solar panels.

curation. **Rajaram S. Sutar:** Investigation, Data curation. **Sanjay Latthe:** Investigation, Data curation. **Ruimin Xing:** Supervision, Conceptualization. **Shanhu Liu:** Writing – review & editing, Project administration, Funding acquisition.

Declaration of competing interest

The authors state that they have no competitive economic interests or personal relationships that may affect the work reported in this paper.

Acknowledgements

We greatly appreciate the support of the National Natural Science Foundation of China (21950410531), Henan province Science and Technology Research Project (242102240045), and the support of the Petro-China Research Institute of Petroleum Exploration & Development (RIPED-2019-CL-186).

Appendix A. Supplementary data

Supplementary data to this article can be found online at https://doi.org/10.1016/j.porgcoat.2025.109674.

Data availability

Data will be made available on request.

References

[1] S. Saher, S. Johnston, R. Esther-Kelvin, J.M. Pringle, D.R. MacFarlane, K. Matuszek, Trimodal thermal energy storage material for renewable energy applications, Nature 636 (2024) 622–626.
[2] P. Tao, G. Ni, C. Song, W. Shang, J. Wu, J. Zhu, G. Chen, T. Deng, Solar-driven interfacial evaporation, Nat. Energy 3 (2018) 1031–1041.
[3] X. Zhu, Z. Xu, S. Zuo, J. Feng, Z. Wang, X. Zhang, K. Zhao, J. Zhang, H. Liu, S. Priya, S.F. Liu, D. Yang, Vapor-fumigation for record efficiency two-dimensional perovskite solar cells with superior stability, Energy Environ. Sci. 11 (2018) 3349–3357.
[4] L. Mi, Y. Wang, X. Fang, X. Qi, L. Chen, H. Cui, Laser-fabricated core-shell cu/Zn-based photocatalytic films with superhydrophilic self-cleaning properties, J. Alloys Compd. 1026 (2025) 180422.
[5] H. Cui, X. Fang, X. Qi, Y. Wang, H. Wang, Z. Zhai, F. Zhang, Q. Hu, J. Liu, Laser-fabricated core-shell Ti/W based photocatalytic films with superhydrophilic self-cleaning properties, Surf Interfaces 61 (2025) 106147.
[6] F. Geyer, M. D'Acunzi, A. Sharifi-Aghili, A. Saal, N. Gao, A. Kaltbeitzel, T.-F. Sloot, R. Berger, H.-J. Butt, D. Vollmer, When and how self-cleaning of superhydrophobic surfaces works, Sci. Adv. 6 (2020) eaaw9727.
[7] A. Lafuma, D. Quere, Superhydrophobic states, Nat. Mater. 2 (2003) 457–460.
[8] X. Liu, H. Zhang, Y. Pan, J. Ma, C. Liu, C. Shen, A transparent polymer-composite film for window energy conservation, Nano-Micro Lett. 17 (2025) 151.
[9] X. Luo, W. Lv, H. Luo, L. Wang, P. Liu, X. Deng, Z. Liu, R. Wei, Z. Xiong, B. Tang, Mass-produced anti-fogging films with excellent performances formed from amphiphilic random copolymers via roll-to-roll coating, Prog. Org. Coat. 200 (2025) 109089.
[10] M. Wang, P. Ma, M. Yin, L. Lu, Y. Lin, X. Chen, W. Jia, X. Cao, P. Chang, D. Li, Scalable production of mechanically robust antireflection film for omnidirectional enhanced flexible thin film solar cells, Adv. Sci. 4 (2017) 1700079.
[11] Y. Yao, K.T. Lee, X. Sheng, N.A. Batara, N. Hong, J. He, L. Xu, M.M. Hussain, H. A. Atwater, N.S. Lewis, R.G. Nuzzo, J.A. Rogers, Porous nanomaterials for ultrabroadband omnidirectional anti-reflection surfaces with applications in high concentration photovoltaics, Adv. Energy Mater. 7 (2016) 1601992.
[12] J. Huang, Z. Ren, Y. Zhang, K. Liu, H. Zhang, H. Tang, C. Yan, Z. Zheng, G. Li, Stretchable ITO-free organic solar cells with intrinsic anti-reflection substrate for high-efficiency outdoor and indoor energy harvesting, Adv. Funct. Mater. 31 (2021) 2010172.
[13] D. Du, F. Wang, D. Zhang, J. Bao, Y. Fan, Y. Guo, W. Shen, H. Wang, One-step synthesis of SiO_2 nanomesh for antireflection and self-cleaning of solar cell, J. Colloid Interface Sci. 630 (2023) 795–803.
[14] J. Wan, W. Wu, Y. Wang, W. Zhou, J. Shao, C. Wan, H. Hou, Sodium alginate/poly (vinyl alcohol)/graphitic carbon nitride composite membrane with excellent anti-fouling properties for efficient oil-water separation, Prog. Org. Coat. 207 (2025) 109352.
[15] K. Ding, X. Zhang, L. Ning, Z. Shao, P. Xiao, A. Ho-Baillie, X. Zhang, J. Jie, Hue tunable, high color saturation and high-efficiency graphene/silicon heterojunction solar cells with MgF_2/ZnS double anti-reflection layer, Nano Energy 46 (2018) 257–265.
[16] C. Ma, L. Wang, X. Fan, J. Liu, Broadband antireflection and hydrophobic CaF_2 film prepared with magnetron sputtering, Appl. Surf. Sci. 560 (2021) 149924.
[17] J.-S. Yu, S. Jung, J.-W. Cho, G.-T. Park, M. Kats, S.-K. Kim, E. Lee, Ultrathin Ge-YF_3 antireflective coating with 0.5% reflectivity on high-index substrate for long-wavelength infrared cameras, Nanophotonics 13 (2024) 4067–4078.
[18] D.F. Rodríguez, P.M. Perillo, M.P. Barrera, High performance TiO_2 nanotubes antireflection coating, Mater. Sci. Semicond. Proc 71 (2017) 427–432.
[19] R.S. Sutar, B. Shi, S.S. Kanchankoti, S.S. Ingole, W.S. Jamadar, A.J. Sayyad, P. B. Khot, K.K. Sadasivuni, S.S. Latthe, S. Liu, A.K. Bhosale, Development of self-cleaning superhydrophobic cotton fabric through silica/PDMS composite coating, Surf Topogr Metrol Prop 11 (2023) 045004.
[20] Z. Zhao, H. Jiang, M. Cheng, S. Wang, S. Sun, C. Li, S. Hu, A multi-strategy coating for Al alloy based on orientationally arranged nanosheets doped SiO_2 coating and corrosion inhibitor loaded porous anodic alumina film, Prog. Org. Coat. 191 (2024) 108419.
[21] J.Y. Huang, G.T. Fei, S.H. Xu, B. Wang, ZnO-SiO_2 composite coating with anti-reflection and photoluminescence properties for improving the solar cell efficiency, Compos. Part B Eng. 251 (2023) 110486.
[22] J. Zhang, J. Yuan, P. Tian, J. Mao, Q. Zhang, Preparation of gradient refractive index films on glass surface and its anti-reflection properties, J. Alloys Compd. 972 (2024) 172831.
[23] Z. Zhang, H. Zhang, H. Zhang, Y. Shao, J. Zhu, Mussel-inspired antimicrobial and antireflective Ag-NPs/PDA/SiO_2 coatings via interfacial functionalization, Chem. Eng. J. 490 (2024) 151434.
[24] S.S. Ingole, R.S. Sutar, P.P. Gaikwad, A.R. Jundle, R.A. Ekunde, S. Liu, S.S. Latthe, A review on transparent superhydrophobic coatings for self-cleaning solar cell panels: its fabrication, robustness and industrial implementation, Surf Interfaces 70 (2025) 106794.
[25] S.S. Latthe, R.S. Sutar, V.S. Kodag, A.K. Bhosale, A.M. Kumar, K. Kumar Sadasivuni, R. Xing, S. Liu, Self - cleaning superhydrophobic coatings: potential industrial applications, Prog. Org. Coat. 128 (2019) 52–58.
[26] G. Socrates, Infrared and Raman Characteristic Group Frequencies: Tables and Charts, 3rd ed, Wiley, 2001.
[27] Y. She, L. Shao, M. Yi, Y. Fang, L. Qin, Y. Liu, X. Wang, K. Wang, Efficient and inexpensive preparation of mesoporous silica microspheres and their highly selective adsorption-cycling performance for Ga(III) in acidic solutions, Chem. Eng. J. 511 (2025) 162007.
[28] R. Lukose, M. Lisker, F. Akhtar, M. Fraschke, T. Grabolla, A. Mai, M. Lukosius, Influence of plasma treatment on SiO_2/Si and Si_3N_4/Si substrates for large-scale transfer of graphene, Sci. Rep. 11 (2021) 13111.
[29] X.D. Wang, W. Wang, J.L. Liu, J.H. Qi, Y. He, Y.F. Wang, W.J. Hu, Y.J. Cheng, K. Chen, Y. Hu, A.Y. Mei, H.W. Han, Reducing optical reflection loss for perovskite solar cells via printable mesoporous SiO_2 antireflection coatings, Adv. Funct. Mater. 32 (2022) 2203872.
[30] Y. Chen, Z. Quan, P. Wang, X. Zhang, H. Ding, B. Li, B. Li, S. Niu, J. Zhang, Z. Han, L. Ren, Bioinspired antireflective and antifogging surface for highly efficient and stable inverted solar cells, ACS Appl. Mater. Interfaces 16 (2024) 65656–65666.
[31] Y. Wu, J. Zeng, Y. Si, M. Chen, L. Wu, Large-area preparation of robust and transparent superomniphobic polymer films, ACS Nano 12 (2018) 10338–10346.
[32] J. Yoon, M. Ryu, H. Kim, G.N. Ahn, S.J. Yim, D.P. Kim, H. Lee, Wet-style superhydrophobic antifogging coatings for optical sensors, Adv. Mater. 32 (2020) 2002710.
[33] K. Manabe, S. Nishizawa, K.-H. Kyung, S. Shiratori, Optical phenomena and antifrosting property on biomimetics slippery fluid-infused antireflective films via layer-by-layer comparison with superhydrophobic and antireflective films, ACS Appl. Mater. Interfaces 6 (2014) 13985–13993.
[34] T. Ren, J. He, Substrate-versatile approach to robust antireflective and superhydrophobic coatings with excellent self-cleaning property in varied environments, ACS Appl. Mater. Interfaces 9 (2017) 34367–34376.
[35] J. Rombaut, S. Martínez, U.M. Matera, P. Mazumder, V. Pruneri, Antireflective multilayer surface with self-cleaning subwavelength structures, ACS Photonics 8 (2021) 894–900.
[36] W. He, J. Ou, F. Wang, S. Lei, X. Fang, W. Li, A. Amirfazli, Transparent and superhydrophobic coating via one-step spraying for cultural relic protection against water and moisture, Colloids Surf. A Physicochem. Eng. Aspects. 662 (2023) 130949.
[37] L. Zhang, J. Xu, Z. Hu, P. Wang, J. Shang, J. Zhou, L. Ren, Antireflective superhydrophobic and robust coating based on chitin nanofibers and methylsilanized silica for outdoor applications, ACS Appl. Mater. Interfaces 16 (2024) 38690–38701.
[38] J.-H. Park, D.-S. Park, B.-D. Hahn, J.-J. Choi, J. Ryu, S.-Y. Choi, J. Kim, W.-H. Yoon, C. Park, Effect of raw powder particle size on microstructure and light transmittance of α-alumina films deposited by granule spray in vacuum, Ceram. Int. 42 (2016) 3584–3590.
[39] M. Du, W. Chen, C. Qian, Z. Chen, G.-L. Chen, H.-Q. Yu, Using rayleigh scattering to correct the inner filter effect of the fluorescence excitation–emission matrix, Anal. Chem. 95 (2023) 12273–12283.
[40] Y. Wang, D.W. Collinson, H. Kwon, R.D. Miller, K. Lionti, K.E. Goodson, R. H. Dauskardt, Linking interfacial bonding and thermal conductivity in molecularly-confined polymer-glass nanocomposites with ultra-high interfacial density, Small 19 (2023) 2301383.
[41] X. Xie, X. Qi, X. Chen, H. Cui, Durable self-cleaning anti-fog and antireflective titanium-based micro–nano structures on glass by laser marker ablation, Surf Interfaces 51 (2024) 104644.
[42] S. Oh, J.W. Cho, J. Lee, J. Han, S.K. Kim, Y. Nam, A scalable haze-free antireflective hierarchical surface with self-cleaning capability, Adv. Sci. 9 (2022) 2202781.